Physics – Uspekhi **51** (9) 899 – 909 (2008)

INSTRUMENTS AND METHODS OF INVESTIGATION PACS numbers: **42.62. – b**, **42.65. – k**, 42.70.Ce

New nonlinear laser effects in α-quartz: generation of a two-octave Stokes and anti-Stokes comb and cascaded lasing in the spectral range of the second and third harmonics

A A Kaminskii, L Bohatý, P Becker, H J Eichler, H Rhee

DOI: 10.1070/PU2008v051n09ABEH006650

Contents

1. **Introduction** 899
2. **Crystallography of the samples** 900
3. **Nonlinear generation effects: multi-octave combs of Stokes and anti-Stokes components and multi-cascaded $\chi^{(3)} \leftrightarrow \chi^{(2)}$ lasing** 900
4. **Raman gain coefficient** 902
5. **SRS-promoting vibration mode of α-quartz** 904
6. **Conclusion** 905

References 908

Abstract. Crystals that are simultaneously $\chi^{(2)}$- and $\chi^{(3)}$-active offer a wide range of possibilities for the generation of new coherent wavelengths of light. Frequency conversion processes such as stimulated Raman scattering, second and third harmonic generation, or parametric sum and difference frequency mixing can be combined effectively in the same noncentrosymmetric crystal in cascaded $\chi^{(3)} \leftrightarrow \chi^{(2)}$ lasing processes. We present several new manifestations of these effects under picosecond laser excitation in α-quartz (SiO_2), the oldest nonlinear-laser crystal. Among them are 45 Stokes and anti-Stokes wavelength comb generation of more than two octaves (from 0.3692 μm to 1.5142 μm) and self-conversion of Raman-generation frequencies into the wavelength region of the second and third harmonics of one-micron pumping via many-step cascaded $\chi^{(3)} \leftrightarrow \chi^{(2)}$ processes.

A A Kaminskii Shubnikov Institute of Crystallography,
Russian Academy of Sciences,
Leninskii prosp. 59, 119333 Moscow, Russian Federation
Tel. (7-499) 135 22 10 (6310). Fax (7-499) 135 10 11
E-mail: kaminalex@mail.ru
L Bohatý, P Becker Institut für Kristallographie, Universität zu Köln,
Zülpicher Str. 49b, D-50674 Köln, Germany
Tel. (+49) 221-470-3154, (+49) 221-470-6104
Fax (+49) 221-470-4963, (+49) 221-470-4963
E-mail: ladislav.bohaty@uni-koeln.de, petra.becker@uni-koeln.de
H J Eichler, H Rhee Institut für Optik and Atomare Physik,
Technische Universität Berlin,
Hardenbergstr. 36, D-10623 Berlin, Germany
Tel. (+49) 30-314-22468, (+49) 30-314-24701. Fax (+49) 30-314-21079
E-mail: eichler@physik.tu-berlin.de, hanjo@physik.tu-berlin.de

Received 29 April 2008
Uspekhi Fizicheskikh Nauk **178** (9) 935 – 946 (2008)
Translated by N V Chernega; edited by A M Semikhatov

1. Introduction

In solid state sciences, α-quartz has frequently played a key role not only due to its easy availability as high-quality large crystals from nature but also due to its special symmetry, which allows the occurrence of a variety of fascinating crystal physical properties. In the field of linear and nonlinear optics, α-quartz has been a research-stimulating material through the last centuries: already in the first decades of the 19th century, detailed measurements of refractive indices on quartz and calcite were used to study anisotropic light propagation.

We recall that *optical activity* was discovered in 1811 by Arago [1] in crystals of α-quartz, and shortly after Fresnel succeeded with a brilliant experiment to verify circular birefringence using prisms of left- and right-handed quartz [2]. Following Brewster's experiments on stress-induced birefringence in optically isotropic media [3], quartz served as one of the pioneering optically anisotropic crystals for the study of the *piezo-optic effect* [4]. The first experimental evidence for the *linear electro-optic effect* was simultaneously provided by Röntgen and by Kundt using α-quartz [5]. A detailed quantitative analysis by Pockels established the existence of the 'true' linear electro-optic effect (the Pockels effect) [6] and corrected the interpretation of Röntgen and Kundt.

The thorough investigation of inelastic light scattering in natural α-quartz by Landsberg and Mandelshtam in 1928 [7] marks the discovery of the *spontaneous Raman effect in solids* (we note that the key publication by Raman, dealing with this scattering effect in fluid media, was presented simultaneously [8]). Throughout many years, the different aspects of Raman scattering in natural and synthetic crystals of α-quartz have been systematically studied by many researchers (for earlier works, see, e.g., Refs [9]).

Soon after the invention of the laser, α-quartz also served as a pioneering crystal in the field of nonlinear optics, where the first optical frequency conversion process via $\chi^{(2)}$

nonlinearity, the *second harmonic generation* (SHG), were proved [10]. Because phase-matched SHG is not possible in α-quartz, the crystals are not used as an SHG material, although the SHG coefficient d_{111}^{SHG} is nearly as high as d_{312}^{SHG} of KDP [11]. But the coefficient $d_{111}^{\mathrm{SHG}} = 0.30$ pm V^{-1} (for $\lambda = 1.064$ μm) [12] of α-quartz is certified and widely used as a standard value for absolute calibration of relative measurements of SHG coefficients that are obtained, for example, using the Maker fringes method.

Crystals of α-quartz were also the first solid-state material in which *stimulated Raman scattering* (SRS) generation based on its second nonlinearity $\chi^{(3)}$ was observed with excitation by the red emission (at the wavelength 0.6943 μm) of a ruby laser [13], only a few years after the discovery of *stimulated Brillouin scattering* in the same material [14].

The interest in α-quartz and its vibration properties is still strong (see, e.g., Refs [15]), for example, for the generation of infrared and teraherz radiation by stimulated polariton emission (see, e.g., Refs [16]). These few examples illustrate that α-quartz has played an eminent and unique role in the birth and progress of nonlinear optics and in the advancement of modern laser physics.

At present, large single crystals of α-quartz of industrial standards are routinely grown by various companies using hydrothermal methods [17] for their main application as the most important piezoelectric single-crystal material. We note that α-quartz was first grown in 1845 by Schafhäutl [18]; it was one of the first successful crystal growth experiments using (moderate) hydrothermal conditions.

In this paper, we report on the first observation of new nonlinear lasing effects in α-quartz where both the cubic $\chi^{(3)}$ and quadratic $\chi^{(2)}$ nonlinearities manifest themselves simultaneously. Furthermore, efficient multi-wavelength cascaded $\chi^{(3)} \leftrightarrow \chi^{(2)}$ generation, among them Raman-induced Stokes and anti-Stokes comb generation over more than two octaves and parametric multi-wave mixing with an involvement of second and third harmonic generation under one-micron picosecond pumping is presented.

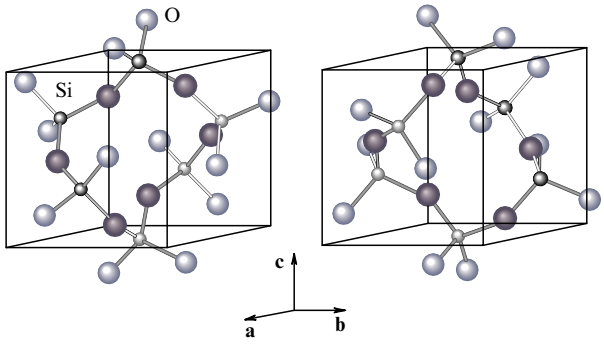

Figure 1. Structure plot of α-quartz showing both enantiomorphic species with the space group $P3_221$ (left side) or $P3_121$ (right side). The unit cell is indicated in both cases. Si atoms are marked with small black spheres and oxygen atoms with larger blue spheres. The contents of the primitive unit cell is indicated by dark color; atoms that do not belong to the primitive unit cell but help to visualize the structural features of α-quartz are marked with pale color.

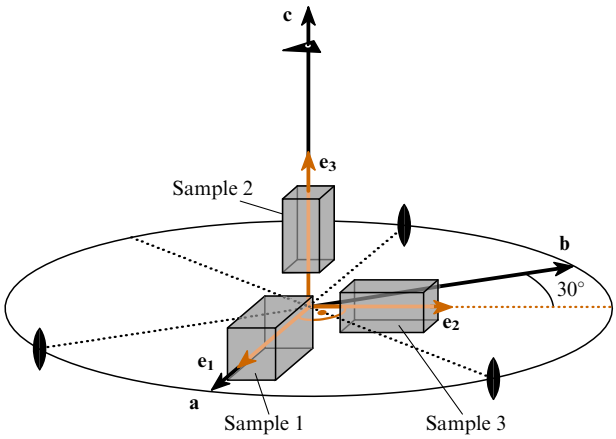

Figure 2. Orientation of samples of α-quartz used in this work. **a**, **b**, and **c** denote the crystallographic axes, $\{\mathbf{e}_i\}$ are the axes of a Cartesian reference system. The three diad symmetry axes and the three-fold axis of the point group 32 are indicated by the standard crystallographic symbols.

2. Crystallography of the samples

α-quartz, the low-temperature/low-pressure crystalline modification of SiO_2, crystallizes in the enantiomorphic point group 32. The structural building units are corner-sharing $[SiO_4]$ tetrahedra that are arranged, depending on the enantiomorphy (space group $P3_121$ or $P3_221$), as either right-handed or left-handed helices, which are linked into a three-dimensional network [19]. In Fig. 1, the structure of α-quartz is presented for left-handed and for right-handed quartz. A quartz crystal of the $P3_221$ symmetry is dextrorotatory in the direction of the optical axis [20, 21]. For our investigations, we used samples that were cut from a commercial, dextro-rotatory large single crystal.

For the indication of the sample orientation, we use a Cartesian coordinate system $\{\mathbf{e}_i\}$ related to the crystallographic system $(\mathbf{a}, \mathbf{b}, \mathbf{c})$ according to the IEEE standard [22], i.e., $\mathbf{e}_1$ is parallel to one of the twofold axes, $\mathbf{e}_2$ is perpendicular to this twofold axis, and $\mathbf{e}_3$ is parallel to the threefold axis of the crystal. Here, the longitudinal piezoelectric constant d_{111} is positive. The samples were prepared for incidence of the pump beam along $\mathbf{e}_1$ with the sample length 59.9 mm, along $\mathbf{e}_2$ with the sample length 54.5 mm, and along $\mathbf{e}_3$ with the sample length 35.8 mm (see Fig. 2). Plane-parallel faces of incidence were polished carefully, but no antireflection coating was applied. A compilation of some selected properties of α-quartz is given in Table 1.

3. Nonlinear generation effects: multi-octave combs of Stokes and anti-Stokes components and multi-cascaded $\chi^{(3)} \leftrightarrow \chi^{(2)}$ lasing

For the excitation of a single-pass (cavity-free) Raman-induced Stokes and anti-Stokes, as well as nonlinear, cascaded $\chi^{(3)} \leftrightarrow \chi^{(2)}$ generation in the UV, visible, and near- and mid-IR range of α-quartz single crystals, we used a modified experimental setup based on a home-made Xe-flashlamp pumped picosecond $Nd^{3+}:Y_3Al_5O_{12}$ laser (master oscillator and amplifier) with an efficient (≈ 25%) external KDP (KH_2PO_4) frequency doubling crystal. Details of the laser system are described in our recent publication [46]. The laser setup can emit at two fundamental wavelengths: $\lambda_{\mathrm{f1}} = 1.06415$ μm (the main inter-Stark generation transition of the $^4F_{3/2} \rightarrow {}^4I_{11/2}$ channel of Nd^{3+} lasants [47], the pulse duration $\tau_{\mathrm{p1}} \approx 100$ ps) and $\lambda_{\mathrm{f2}} = 0.53207$ μm (SHG, $\tau_{\mathrm{p2}} \approx 80$ ps). The nearly Gaussian beam of the

Table 1. Some selected physical properties of α-quartz single crystals at room temperature (unless indicated otherwise); errors are given in parentheses (the table continues on the next page).

Space group [19]	D_3^4-P3$_1$21 (No. 152) or D_3^6-P3$_2$21 (No. 154)
Unit cell parameters, Å [23]	$a = 4.91344(4)$, $c = 5.40524(8)$
Formula units per cell [19]	$Z = 3$
Experimental density (g cm^{-3}) (at 0 °C) [24]	$\rho_{exp} = 2.65068(23)$
Site symmetry of atoms [19]	Si: 2 (C_2), O: 1 (C_1)
Method of crystal growth	Hydrothermal [17]; crystals available commercially
Hardness: Mohs scale Knoop scale (kg mm^{-2})	7 ≈ 740
Melting temperature,[1] K [25, 26]	1996(5)
Thermal conductivity coefficients[2] κ_{ij}, W m^{-1} K^{-1} [27]	$\kappa_{11} = 6.2(3)$, $\kappa_{33} = 10.4(5)$
Optical character	Uniaxial positive: $n_e > n_o$
Optical transparency range,[3] μm [28]	≈ 0.19– ≈ 3.6
Band-gap energy, eV [29]	≈ 8.30
Optical damage threshold, GW cm^{-2} (at $\lambda = 0.6943$ μm) [30]	≈ 28(5)
Refractive indices (dispersion equation)[4] [31]	$n^2(\lambda) = A + \frac{B}{\lambda^2 - C} + \frac{D}{\lambda^2 - E} + \frac{127.2}{\lambda^2 - 108}$
Optical activity, deg mm^{-1} [32]: at $\lambda = 0.481$ μm at $\lambda = 0.535$ μm at $\lambda = 0.589$ μm at $\lambda = 0.636$ μm at $\lambda = 0.940$ μm at $\lambda = 1.100$ μm at $\lambda = 1.342$ μm	 33.52 26.67 21.75 18.48 8.14 5.836 3.890

[1] Melting temperature of high-cristobalite (stable modification of crystalline SiO_2 at high temperatures and ambient pressure); note that β-quartz can be superheated through the cristobalite stability range, with a metastable melting temperature at ≈ 1696(50)K [25, 26].
[2] Similar values ($\kappa_{11} \approx 7$ W m^{-1} K^{-1} and $\kappa_{33} \approx 12$ W m^{-1} K^{-1}) are given in [42].
[3] Transparency range at 0.5 transmittance level for a 10-mm long c-axis cut crystal [28] (see also Fig. 3).
[4] Dispersion coefficients, λ is in μm (the subscripts 'o' and 'e' stand for 'ordinary' and 'extraordinary')

	A	B	C	D	E
n_o	3.53445	0.008067	0.0127493	0.002682	0.000974
n_e	3.5612557	0.00844614	0.0127493	0.00276113	0.000974

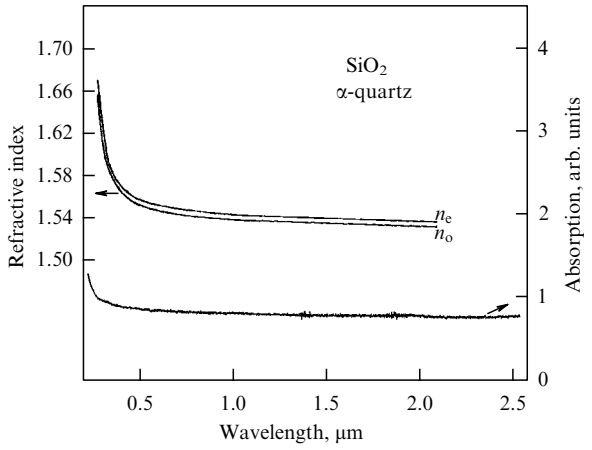

Figure 3. Room-temperature wavelength dispersion of refractive indices of α-quartz (data taken from [31]) and a portion of its absorption spectrum in the range from UV to near-IR recorded with a (001) plate 1.34 mm thick without antireflection coating.

fundamental (pump) emission is focused into our oriented α-quartz samples with a lens ($f = 25$ cm), resulting in the beam waist diameter about 160 μm. The spectral composition of the nonlinear-lasing components of the studied crystals, which range from the UV to the mid-IR region, was dispersed with a grating monochromator in the Czerny–Turner arrangement (McPherson Model 270 with a grating of 150 lines/mm) and recorded by two Hamamatsu linear image sensors based on charge-coupled devices Si-CCD (S3923-1024Q) and InGaAs-CCD (G9204-512D). Selected typical results of Raman-induced and cascaded $\chi^{(3)} \leftrightarrow \chi^{(2)}$ lasing spectra of α-quartz, recorded in specific excitation geometries, together with the results of their analysis, are shown in Figs 4–8 and summarized in Table 2.

As can be seen from Fig. 4 and Fig. 8a, under one micron picosecond pumping (peak power on the MW level) using the excitation geometry $\mathbf{e}_1(\mathbf{e}_2, \mathbf{e}_2)\mathbf{e}_1$, a comb of 45 wavelengths (6 Stokes, 38 anti-Stokes, and pumping emission) with strictly equally separated ($\omega_{SRS} = 465.5$ cm^{-1}) lines, spanning from the visible ($\lambda_{ASt38} = 0.3692$ μm) to the mid-IR region ($\lambda_{St6} = 1.5142$ μm), was excited by direct SRS and by the

Table 1 (continuation)

Nonlinear refractive indices n_2, 10^{-13} cm^3 erg) (at $\lambda = 1.064$ μm) [33]	1.16 ($\parallel c$-axis); 1.12 ($\perp c$-axis)
Phase matching conditions for SHG	No phase matching possible
Nonlinearity	$\chi^{(2)} + \chi^{(3)}$
Nonlinear coefficients for SHG d_{ijk}^{SHG}, pm V^{-1} (at $\lambda = 1.064$ μm) [12, 34]	$d_{111}^{\mathrm{SHG}} = 0.30,\ d_{123}^{\mathrm{SHG}} = -0.0045$
Electro-optic constants r_{ijk}^{σ}, pm V^{-1} (at constant stress, $\lambda = 0.633$ μm) [35]	$r_{111}^{\sigma} = -0.481(8),\ r_{231}^{\sigma} = -0.235(10)$
Photoelastic constants p_{ijkl} (at $\lambda = 0.5893$ μm) [36]	$p_{1111} = 0.16,\ p_{1122} = 0.27,\ p_{1133} = 0.27,\ p_{3311} = 0.29,\ p_{3333} = 0.10,$ $p_{1123} = -0.030,\ p_{2311} = -0.047,\ p_{2323} = -0.079$
Low-frequency relative dielectric constants $\varepsilon_{ij}^{\mathrm{r}}$ (at constant stress) [37]	$\varepsilon_{11}^{\mathrm{r}} = 4.5208(10),\ \varepsilon_{33}^{\mathrm{r}} = 4.6368(10)$
Thermal expansion coefficients, 10^{-6} K^{-1} [38]	$\alpha_{11} = 13.87,\ \alpha_{33} = 7.62$
Piezoelectric coefficients[5] d_{ijk}, pm V^{-1} [35, 39]	$d_{111} = 2.31(1),\ d_{123} = -0.369(13)$
Elastic constants[6] c_{ijkl}, GPa [41]	$c_{1111} = 86.790,\ c_{1122} = 6.790,\ c_{1133} = 12.01,$ $c_{3333} = 105.787,\ c_{1123} = 18.116,\ c_{2323} = 58.212$
Linewidth of SRS-related line in spontaneous Raman scattering spectrum,[7] cm^{-1}	$\Delta\nu_{\mathrm{R}} = 6.7 \pm 0.3$
SRS-promoting vibration modes,[8] cm^{-1}	$\omega_{\mathrm{SRS}} = 465.5 \pm 1.0$
Phonon spectrum extension,[9] cm^{-1}	≈ 1250

[5] See also a compilation of piezoelectric data in [40].
[6] See also a compilation of elastic data in [43].
[7] Several earlier precise measurements of the $\Delta\nu_{\mathrm{R}}$ value for vibration transition related to room-temperature SRS lasing in α-quartz are known [44].
[8] At cryogenic temperature, SRS generation has been found with frequency shifts 128 – 132 cm^{-1} (E-mode) and 466 – 468 cm^{-1} (A_1-mode) (see, e.g., Refs [13, 45]).
[9] From first-order spontaneous Raman scattering spectra (see, e.g., [9]).

parametric process of Raman-induced four-wave mixing (RFWM). This comb covers the frequency interval of 20,481 cm^{-1}, which is more than two octaves. This range can be extended by using a biphoton ultrashort excitation in transient conditions, where $\tau_{\mathrm{p}} < T_2$, if the waves of the fundamental pumping ($\lambda_{\mathrm{fl}} = 1.06415$ μm) and the first Stokes component ($\lambda_{\mathrm{St1}} = 1.1196$ μm) satisfy phase matching conditions for RFWM. In this pumping scheme, a majority of the number of excited Stokes and anti-Stokes components could probably be coherent and propagate colinearly. In addition to the broadband lasing comb arising from one-micron picosecond pumping, self-frequency conversion processes generated SHG and THG lines and cascaded many wavelength lasing effects in the deep blue and green spectral region (see Figs 6 – 8), which might increase the interest in this material. These effects, however, are not found exclusively in α-quartz [50]; they have been observed in several inorganic and organic noncentrosymmetric crystals such as β-$LaBGeO_5$, β′-$Gd_2(MoO_4)_3$, and $Ca_4GdO(BO_3)_3$ [51], β-BaB_2O_4 [52], $C_{16}H_{15}N_3O_4$ 4′-Nitrobenzylidene-3-Acetamino-4-Methoxyaniline, MNBA) [53], BiB_3O_6 [54], $C_{15}H_{19}N_3O_2$ (2-Adamantylamino-5-Nitropyridine, AANP) [55], $LiGeBO_4$ [56], $Y(HCOO)_3 \cdot 2H_2O$ [57], $CsLiMoO_4$ and $CsLiMoO_4 \cdot 1/3H_2O$ [58], $Li_2SO_4 \cdot H_2O$ [59], $Li_2B_4O_7$ [60], PbB_4O_7 [61], and $LaBO_2MoO_4$ [62]), as well as $NH_4H_2PO_4$ (ADP) and $ND_4D_2PO_4$ (DADP) [46].

It is noteworthy that the Raman-induced $\chi^{(3)}$ and $\chi^{(2)}$ sideband radiation and parametric anti-Stokes SRS lasing is emitted into a relatively small solid angle and partly even collinearly, which is mostly not in agreement with the geometric requirements of phase matching, e.g., for SHG, SFM, or RFWM, calculated from refractive indices and their dispersion. This observed phenomenon could probably be explained by the generation of the resulting sideband radiation or SHG within one coherence length of the concrete conversion process under strong pumping power. Our observation of relatively strong SHG in α-quartz (where the SHG phase matching is not realizable), described in the present work, could corroborate this model. Alternatively, in a more speculative model, a modification of the refractive indices by a strong pumping wave (due to the optical Kerr effect) could create self-organization of the phase matching conditions.

It is hoped that the experimental knowledge collected so far is already a sufficient base for the development of a realistic theoretical model of these interesting nonlinear-laser manifestations, which promise new possibilities for applications. We emphasize that first steps in understanding this new phenomenon were already made in studies of parametric anti-Stokes SRS lasing in solid hydrogen, as well as of broadband coherent light generation in a lead tungstate ($PbWO_4$) crystal (see, e.g., [63]).

4. Raman gain coefficient

In our measurements, the SRS process in α-quartz was essentially realized with steady-state (ss) conditions, because the laser pump pulse durations $\tau_{\mathrm{p1}} \approx 100$ ps and $\tau_{\mathrm{p2}} \approx 80$ ps were much longer than the phonon relaxation time $T_2 = (\pi\Delta\nu_{\mathrm{R}})^{-1} \approx 1.6$ ps (here, $\Delta\nu_{\mathrm{R}} \approx 6.7$ cm^{-1}; see Fig. 9 and Table 1) of the SRS-promoting vibration transition of the crystal (with $\omega_{\mathrm{SRS}} = 465.5$ cm^{-1}). Therefore, we can roughly estimate the first Stokes Raman gain coefficient $g_{\mathrm{ssR}}^{\mathrm{St1}}$ in the studied crystal at the $\lambda_{\mathrm{St1}} = 1.1196$ μm wavelength with the excitation geometry $\mathbf{e}_1(\mathbf{e}_2, \mathbf{e}_2)\mathbf{e}_1$. This was done indirectly by the sufficiently tested method based on the well-known ratio $g_{\mathrm{ssR}}^{\mathrm{St1}} I_{\mathrm{p}}^{\mathrm{thr}} l_{\mathrm{SRS}} \approx 30$ (see, e.g., [64]) and a comparison of the 'threshold' pump intensity $I_{\mathrm{p}}^{\mathrm{thr}}$ of the confidently measurable

Table 2. Room-temperature spectral composition of nonlinear $\chi^{(2)}$- and $\chi^{(3)}$-lasing: SRS, Raman-induced four-wave mixing (RFWM), cascaded self-frequency doubling and tripling in α-quartz with picosecond $Nd^{3+}:Y_3Al_5O_{12}$-laser excitation under steady-state condition at two fundamental wavelengths $\lambda_{f1} = 1.06415$ μm and $\lambda_{f2} = 0.53207$ μm (SHG).

Pumping condition		Raman-induced nonlinear lasing		
λ_f, μm	Excitation geometry [1]	Wavelength, [2] μm	Line [3]	Nonlinear-lasing attribution [4]
1.06415	$\mathbf{e}_1(\mathbf{e}_2,\mathbf{e}_2)\mathbf{e}_1$ (see Fig. 4)	0.5216	ASt_{21}	$\omega_{f1} + 21\omega_{SRS}$
		0.5345	ASt_{20}	$\omega_{f1} + 20\omega_{SRS}$
		0.5482	ASt_{19}	$\omega_{f1} + 19\omega_{SRS}$
		0.5625	ASt_{18}	$\omega_{f1} + 18\omega_{SRS}$
		0.5777	ASt_{17}	$\omega_{f1} + 17\omega_{SRS}$
		0.5936	ASt_{16}	$\omega_{f1} + 16\omega_{SRS}$
		0.6105	ASt_{15}	$\omega_{f1} + 15\omega_{SRS}$
		0.6284	ASt_{14}	$\omega_{f1} + 14\omega_{SRS}$
		0.6473	ASt_{13}	$\omega_{f1} + 13\omega_{SRS}$
		0.6674	ASt_{12}	$\omega_{f1} + 12\omega_{SRS}$
		0.6888	ASt_{11}	$\omega_{f1} + 11\omega_{SRS}$
		0.7116	ASt_{10}	$\omega_{f1} + 10\omega_{SRS}$
		0.7360	ASt_9	$\omega_{f1} + 9\omega_{SRS}$
		0.7621	ASt_8	$\omega_{f1} + 8\omega_{SRS}$
		0.7902	ASt_7	$\omega_{f1} + 7\omega_{SRS}$
		0.8203	ASt_6	$\omega_{f1} + 6\omega_{SRS}$
		0.8529	ASt_5	$\omega_{f1} + 5\omega_{SRS}$
		0.8882	ASt_4	$\omega_{f1} + 4\omega_{SRS}$
		0.9265	ASt_3	$\omega_{f1} + 3\omega_{SRS}$
		0.9684	ASt_2	$\omega_{f1} + 2\omega_{SRS}$
		1.0139	ASt_1	$\omega_{f1} + \omega_{SRS}$
		1.06415	λ_{f1}	ω_{f1}
		1.1196	St_1	$\omega_{f1} - \omega_{SRS}$
		1.1812	St_2	$\omega_{f1} - 2\omega_{SRS}$
		1.2499	St_3	$\omega_{f1} - 3\omega_{SRS}$
		1.3271	St_4	$\omega_{f1} - 4\omega_{SRS}$
		1.4145	St_5	$\omega_{f1} - 5\omega_{SRS}$
		1.5142	St_6	$\omega_{f1} - 6\omega_{SRS}$
0.53207	$\mathbf{e}_1(\mathbf{e}_2,\mathbf{e}_2)\mathbf{e}_1$ (see Fig. 5)	0.4181	ASt_{11}	$\omega_{f2} + 11\omega_{SRS}$
		0.4264	ASt_{10}	$\omega_{f2} + 10\omega_{SRS}$
		0.4351	ASt_9	$\omega_{f2} + 9\omega_{SRS}$
		0.4441	ASt_8	$\omega_{f2} + 8\omega_{SRS}$
		0.4534	ASt_7	$\omega_{f2} + 7\omega_{SRS}$
		0.4632	ASt_6	$\omega_{f2} + 6\omega_{SRS}$
		0.4734	ASt_5	$\omega_{f2} + 5\omega_{SRS}$
		0.4841	ASt_4	$\omega_{f2} + 4\omega_{SRS}$
		0.4953	ASt_3	$\omega_{f2} + 3\omega_{SRS}$
		0.5070	ASt_2	$\omega_{f2} + 2\omega_{SRS}$
		0.5192	ASt_1	$\omega_{f2} + \omega_{SRS}$
		0.53207	λ_{f2}	ω_{f2}
		0.5456	St_1	$\omega_{f2} - \omega_{SRS}$
		0.5598	St_2	$\omega_{f2} - 2\omega_{SRS}$
		0.5748	St_3	$\omega_{f2} - 3\omega_{SRS}$
		0.5906	St_4	$\omega_{f2} - 4\omega_{SRS}$
		0.6073	St_5	$\omega_{f2} - 5\omega_{SRS}$
		0.6249	St_6	$\omega_{f2} - 6\omega_{SRS}$
		0.6437	St_7	$\omega_{f2} - 7\omega_{SRS}$
1.06415	$\mathbf{e}_2(\mathbf{e}_1,\mathbf{e}_1)\mathbf{e}_2$ (see Fig. 6)	0.4734	$\lambda_{S\text{-}SFM}(\lambda_{f1},\lambda_{ASt5})$	$\omega_{f1} + (\omega_{f1} + 5\omega_{SRS})$
		0.4841	$\lambda_{S\text{-}SFM}(\lambda_{f1},\lambda_{ASt4})$	$\omega_{f1} + (\omega_{f1} + 4\omega_{SRS})$
		0.4953	$\lambda_{S\text{-}SFM}(\lambda_{f1},\lambda_{ASt3})$	$\omega_{f1} + (\omega_{f1} + 3\omega_{SRS})$
		0.5070	$\lambda_{S\text{-}SFM}(\lambda_{f1},\lambda_{ASt2})$	$\omega_{f1} + (\omega_{f1} + 2\omega_{SRS})$
		0.5192	$\lambda_{S\text{-}SFM}(\lambda_{f1},\lambda_{ASt1})$	$\omega_{f1} + (\omega_{f1} + \omega_{SRS})$
		0.53207	SHG [5]	$2\omega_{f1}$
		0.5456	$\lambda_{S\text{-}SFM}(\lambda_{f1},\lambda_{St1})$	$\omega_{f1} + (\omega_{f1} - \omega_{SRS})$
		0.5598	$\lambda_{S\text{-}SFM}(\lambda_{f1},\lambda_{St2})$	$\omega_{f1} + (\omega_{f1} - 2\omega_{SRS})$
		0.5748	$\lambda_{S\text{-}SFM}(\lambda_{f1},\lambda_{St3})$	$\omega_{f1} + (\omega_{f1} - 3\omega_{SRS})$
		0.5906	$\lambda_{S\text{-}SFM}(\lambda_{f1},\lambda_{St4})$	$\omega_{f1} + (\omega_{f1} - 4\omega_{SRS})$
		0.5936	ASt_{16}	$\omega_{f1} + 16\omega_{SRS}$
		0.6105	ASt_{15}	$\omega_{f1} + 15\omega_{SRS}$
		0.6284	ASt_{14}	$\omega_{f1} + 14\omega_{SRS}$
		0.6473	ASt_{13}	$\omega_{f1} + 13\omega_{SRS}$
		0.6674	ASt_{12}	$\omega_{f1} + 12\omega_{SRS}$
		0.6888	ASt_{11}	$\omega_{f1} + 11\omega_{SRS}$
		0.7116	ASt_{10}	$\omega_{f1} + 10\omega_{SRS}$
		0.7360	ASt_9	$\omega_{f1} + 9\omega_{SRS}$
		0.7621	ASt_8	$\omega_{f1} + 8\omega_{SRS}$
		0.7902	ASt_7	$\omega_{f1} + 7\omega_{SRS}$
		0.8203	ASt_6	$\omega_{f1} + 6\omega_{SRS}$
		0.8529	ASt_5	$\omega_{f1} + 5\omega_{SRS}$
		0.8882	ASt_4	$\omega_{f1} + 4\omega_{SRS}$
		0.9265	ASt_3	$\omega_{f1} + 3\omega_{SRS}$
		0.9684	ASt_2	$\omega_{f1} + 2\omega_{SRS}$
		1.0139	ASt_1	$\omega_{f1} + \omega_{SRS}$
		1.06415	λ_{f1}	ω_{f1}
		1.1196	St_1	$\omega_{f1} - \omega_{SRS}$
		1.1812	St_2	$\omega_{f1} - 2\omega_{SRS}$
		1.2499	St_3	$\omega_{f1} - 3\omega_{SRS}$
		1.3271	St_4	$\omega_{f1} - 4\omega_{SRS}$
		1.4145	St_5	$\omega_{f1} - 5\omega_{SRS}$
1.06415	$\mathbf{e}_3(\mathbf{e}_2,\mathbf{e}_2)\mathbf{e}_3$ (see Fig. 7) [6]	0.4953	ASt_3	$2\omega_{f1} + 3\omega_{SRS}$
		0.5070	ASt_2	$2\omega_{f1} + 2\omega_{SRS}$
		0.5192	ASt_1	$2\omega_{f1} + \omega_{SRS}$
		0.53207	SHG [5]	$2\omega_{f1}$
		0.5456	St_1	$2\omega_{f1} - \omega_{SRS}$
		0.5598	St_2	$2\omega_{f1} - 2\omega_{SRS}$
		0.5748	St_3	$2\omega_{f1} - 3\omega_{SRS}$
		0.5906	St_4	$2\omega_{f1} - 4\omega_{SRS}$
		0.6105	ASt_{15}	$\omega_{f1} + 15\omega_{SRS}$
		0.6284	ASt_{14}	$\omega_{f1} + 14\omega_{SRS}$
		0.6473	ASt_{13}	$\omega_{f1} + 13\omega_{SRS}$
		0.6674	ASt_{12}	$\omega_{f1} + 12\omega_{SRS}$
		0.6888	ASt_{11}	$\omega_{f1} + 11\omega_{SRS}$
		0.7116	ASt_{10}	$\omega_{f1} + 10\omega_{SRS}$
		0.7360	ASt_9	$\omega_{f1} + 9\omega_{SRS}$
		0.7621	ASt_8	$\omega_{f1} + 8\omega_{SRS}$
		0.7902	ASt_7	$\omega_{f1} + 7\omega_{SRS}$
		0.8203	ASt_6	$\omega_{f1} + 6\omega_{SRS}$
		0.8529	ASt_5	$\omega_{f1} + 5\omega_{SRS}$
		0.8882	ASt_4	$\omega_{f1} + 4\omega_{SRS}$
		0.9265	ASt_3	$\omega_{f1} + 3\omega_{SRS}$
		0.9684	ASt_2	$\omega_{f1} + 2\omega_{SRS}$
		1.0139	ASt_1	$\omega_{f1} + \omega_{SRS}$
		1.06415	λ_{f1}	ω_{f1}
		1.1196	St_1	$\omega_{f1} - \omega_{SRS}$
		1.1812	St_2	$\omega_{f1} - 2\omega_{SRS}$
1.06415	$\mathbf{e}_1(\mathbf{e}_2,\mathbf{e}_2)\mathbf{e}_1$ (see Fig. 8a)	0.3692	ASt_{38}	$\omega_{f1} + 38\omega_{SRS}$
		0.3756	ASt_{37}	$\omega_{f1} + 37\omega_{SRS}$
		0.3823	ASt_{36}	$\omega_{f1} + 36\omega_{SRS}$
		0.3893	ASt_{35}	$\omega_{f1} + 35\omega_{SRS}$
		0.3964	ASt_{34}	$\omega_{f1} + 34\omega_{SRS}$
		0.4039	ASt_{33}	$\omega_{f1} + 33\omega_{SRS}$
		0.4116	ASt_{32}	$\omega_{f1} + 32\omega_{SRS}$
		0.4197	ASt_{31}	$\omega_{f1} + 31\omega_{SRS}$
		0.4280	ASt_{30}	$\omega_{f1} + 30\omega_{SRS}$
		0.4367	ASt_{29}	$\omega_{f1} + 29\omega_{SRS}$
		0.4458	ASt_{28}	$\omega_{f1} + 28\omega_{SRS}$
		0.4552	ASt_{27}	$\omega_{f1} + 27\omega_{SRS}$
		0.4651	ASt_{26}	$\omega_{f1} + 26\omega_{SRS}$
		0.4754	ASt_{25}	$\omega_{f1} + 25\omega_{SRS}$
		0.4862	ASt_{24}	$\omega_{f1} + 24\omega_{SRS}$
		0.4974	ASt_{23}	$\omega_{f1} + 23\omega_{SRS}$
		0.5092	ASt_{22}	$\omega_{f1} + 22\omega_{SRS}$
		0.5216	ASt_{21}	$\omega_{f1} + 21\omega_{SRS}$
		0.5345	ASt_{20}	$\omega_{f1} + 20\omega_{SRS}$
		0.5482	ASt_{19}	$\omega_{f1} + 19\omega_{SRS}$

Table 2 (continuation)

Pumping condition		Raman-induced nonlinear lasing		
λ_f, μm	Excitation geometry [1]	Wavelength, [2] μm	Line [3]	Nonlinear-lasing attribution [4]
		0.6473	ASt_{13}	$\omega_{f1} + 13\omega_{SRS}$
		0.6674	ASt_{12}	$\omega_{f1} + 12\omega_{SRS}$
		0.6888	ASt_{11}	$\omega_{f1} + 11\omega_{SRS}$
		0.7116	ASt_{10}	$\omega_{f1} + 10\omega_{SRS}$
		0.7360	ASt_9	$\omega_{f1} + 9\omega_{SRS}$
		0.7621	ASt_8	$\omega_{f1} + 8\omega_{SRS}$
		0.7902	ASt_7	$\omega_{f1} + 7\omega_{SRS}$
		0.8203	ASt_6	$\omega_{f1} + 6\omega_{SRS}$
		0.8529	ASt_5	$\omega_{f1} + 5\omega_{SRS}$
		0.8882	ASt_4	$\omega_{f1} + 4\omega_{SRS}$
		0.9265	ASt_3	$\omega_{f1} + 3\omega_{SRS}$
		0.9684	ASt_2	$\omega_{f1} + 2\omega_{SRS}$
		1.0139	ASt_1	$\omega_{f1} + \omega_{SRS}$
		1.06415	λ_{f1}	ω_{f1}
		1.1196	St_1	$\omega_{f1} - \omega_{SRS}$
		1.1812	St_2	$\omega_{f1} - 2\omega_{SRS}$
		1.2499	St_3	$\omega_{f1} - 3\omega_{SRS}$
		1.3271	St_4	$\omega_{f1} - 4\omega_{SRS}$
		1.4145	St_5	$\omega_{f1} - 5\omega_{SRS}$
1.06415	$\mathbf{e}_3(\mathbf{e}_2,\mathbf{e}_2)\mathbf{e}_3$ (see Fig. 7) [6]	0.4953	ASt_3	$2\omega_{f1} + 3\omega_{SRS}$
		0.5070	ASt_2	$2\omega_{f1} + 2\omega_{SRS}$
		0.5192	ASt_1	$2\omega_{f1} + \omega_{SRS}$
		0.53207	SHG [5]	$2\omega_{f1}$
		0.5456	St_1	$2\omega_{f1} - \omega_{SRS}$
		0.5598	St_2	$2\omega_{f1} - 2\omega_{SRS}$
		0.5748	St_3	$2\omega_{f1} - 3\omega_{SRS}$
		0.5906	St_4	$2\omega_{f1} - 4\omega_{SRS}$
		0.6105	ASt_{15}	$\omega_{f1} + 15\omega_{SRS}$
		0.6284	ASt_{14}	$\omega_{f1} + 14\omega_{SRS}$
		0.6473	ASt_{13}	$\omega_{f1} + 13\omega_{SRS}$
		0.6674	ASt_{12}	$\omega_{f1} + 12\omega_{SRS}$
		0.6888	ASt_{11}	$\omega_{f1} + 11\omega_{SRS}$
		0.7116	ASt_{10}	$\omega_{f1} + 10\omega_{SRS}$
		0.7360	ASt_9	$\omega_{f1} + 9\omega_{SRS}$
		0.7621	ASt_8	$\omega_{f1} + 8\omega_{SRS}$
		0.7902	ASt_7	$\omega_{f1} + 7\omega_{SRS}$
		0.8203	ASt_6	$\omega_{f1} + 6\omega_{SRS}$
		0.8529	ASt_5	$\omega_{f1} + 5\omega_{SRS}$
		0.8882	ASt_4	$\omega_{f1} + 4\omega_{SRS}$
		0.9265	ASt_3	$\omega_{f1} + 3\omega_{SRS}$
		0.9684	ASt_2	$\omega_{f1} + 2\omega_{SRS}$
		1.0139	ASt_1	$\omega_{f1} + \omega_{SRS}$
		1.06415	λ_{f1}	ω_{f1}
		1.1196	St_1	$\omega_{f1} - \omega_{SRS}$
		1.1812	St_2	$\omega_{f1} - 2\omega_{SRS}$
1.06415	$\mathbf{e}_1(\mathbf{e}_2,\mathbf{e}_2)\mathbf{e}_1$ (see Fig. 8a)	0.3692	ASt_{38}	$\omega_{f1} + 38\omega_{SRS}$
		0.3756	ASt_{37}	$\omega_{f1} + 37\omega_{SRS}$
		0.3823	ASt_{36}	$\omega_{f1} + 36\omega_{SRS}$
		0.3893	ASt_{35}	$\omega_{f1} + 35\omega_{SRS}$
		0.3964	ASt_{34}	$\omega_{f1} + 34\omega_{SRS}$
		0.4039	ASt_{33}	$\omega_{f1} + 33\omega_{SRS}$
		0.4116	ASt_{32}	$\omega_{f1} + 32\omega_{SRS}$
		0.4197	ASt_{31}	$\omega_{f1} + 31\omega_{SRS}$
		0.4280	ASt_{30}	$\omega_{f1} + 30\omega_{SRS}$
		0.4367	ASt_{29}	$\omega_{f1} + 29\omega_{SRS}$
		0.4458	ASt_{28}	$\omega_{f1} + 28\omega_{SRS}$
		0.4552	ASt_{27}	$\omega_{f1} + 27\omega_{SRS}$
		0.4651	ASt_{26}	$\omega_{f1} + 26\omega_{SRS}$
		0.4754	ASt_{25}	$\omega_{f1} + 25\omega_{SRS}$
		0.4862	ASt_{24}	$\omega_{f1} + 24\omega_{SRS}$
		0.4974	ASt_{23}	$\omega_{f1} + 23\omega_{SRS}$
		0.5092	ASt_{22}	$\omega_{f1} + 22\omega_{SRS}$
		0.5216	ASt_{21}	$\omega_{f1} + 21\omega_{SRS}$
		0.5345	ASt_{20}	$\omega_{f1} + 20\omega_{SRS}$
		0.5482	ASt_{19}	$\omega_{f1} + 19\omega_{SRS}$

Table 2 (continuation)

Pumping condition		Raman-induced nonlinear lasing		
λ_f, μm	Excitation geometry [1]	Wavelength, [2] μm	Line [3]	Nonlinear-lasing attribution [4]
		0.5625	ASt_{18}	$\omega_{fl} + 18\omega_{SRS}$
		0.5777	ASt_{17}	$\omega_{fl} + 17\omega_{SRS}$
		0.5936	ASt_{16}	$\omega_{fl} + 16\omega_{SRS}$
		0.6105	ASt_{15}	$\omega_{fl} + 15\omega_{SRS}$
		0.6284	ASt_{14}	$\omega_{fl} + 14\omega_{SRS}$
		0.6473	ASt_{13}	$\omega_{fl} + 13\omega_{SRS}$
		0.6674	ASt_{12}	$\omega_{fl} + 12\omega_{SRS}$
		0.6888	ASt_{11}	$\omega_{fl} + 11\omega_{SRS}$
		0.7116	ASt_{10}	$\omega_{fl} + 10\omega_{SRS}$
1.06415	$\mathbf{e}_2(\mathbf{e}_1, \mathbf{e}_1)\mathbf{e}_2$ (see Fig. 8b)	0.3547	THG [7]	$3\omega_{fl}$
		0.4280	ASt_{30}	$\omega_{fl} + 30\omega_{SRS}$
		0.4367	ASt_{29}	$\omega_{fl} + 29\omega_{SRS}$
		0.4458	ASt_{28}	$\omega_{fl} + 28\omega_{SRS}$
		0.4552	ASt_{27}	$\omega_{fl} + 27\omega_{SRS}$
		0.4651	ASt_{26}	$\omega_{fl} + 26\omega_{SRS}$
		0.4754	ASt_{25}	$\omega_{fl} + 25\omega_{SRS}$
		0.4862	ASt_{24}	$\omega_{fl} + 24\omega_{SRS}$
		0.4974	ASt_{23}	$\omega_{fl} + 23\omega_{SRS}$
		0.5070	$\lambda_{S\text{-}SFM}(\lambda_{fl}, \lambda_{ASt2})$	$\omega_{fl} + (\omega_{fl} + 2\omega_{SRS})$
		0.5092	ASt_{22}	$\omega_{fl} + 22\omega_{SRS}$
		0.5192	$\lambda_{S\text{-}SFM}(\lambda_{fl}, \lambda_{ASt1})$	$\omega_{fl} + (\omega_{fl} + \omega_{SRS})$
		0.5216	ASt_{21}	$\omega_{fl} + 21\omega_{SRS}$
		0.53207	SHG [5]	$2\omega_{fl}$
		0.5345	ASt_{20}	$\omega_{fl} + 20\omega_{SRS}$
		0.5456	$\lambda_{S\text{-}SFM}(\lambda_{fl}, \lambda_{St1})$	$\omega_{fl} + (\omega_{fl} - \omega_{SRS})$
		0.5482	ASt_{19}	$\omega_{fl} + 19\omega_{SRS}$
		0.5598	$\lambda_{S\text{-}SFM}(\lambda_{fl}, \lambda_{St2})$	$\omega_{fl} + (\omega_{fl} - 2\omega_{SRS})$
		0.5625	ASt_{18}	$\omega_{fl} + 18\omega_{SRS}$
		0.5748	$\lambda_{S\text{-}SFM}(\lambda_{fl}, \lambda_{St3})$	$\omega_{fl} + (\omega_{fl} - 3\omega_{SRS})$
		0.5777	ASt_{17}	$\omega_{fl} + 17\omega_{SRS}$
		0.5906	$\lambda_{S\text{-}SFM}(\lambda_{fl}, \lambda_{St4})$	$\omega_{fl} + (\omega_{fl} - 4\omega_{SRS})$
		0.5936	ASt_{16}	$\omega_{fl} + 16\omega_{SRS}$
		0.6073	$\lambda_{S\text{-}SFM}(\lambda_{fl}, \lambda_{St5})$	$\omega_{fl} + (\omega_{fl} - 5\omega_{SRS})$
		0.6105	ASt_{15}	$\omega_{fl} + 15\omega_{SRS}$
		0.6284	ASt_{14}	$\omega_{fl} + 14\omega_{SRS}$
		0.6473	ASt_{13}	$\omega_{fl} + 13\omega_{SRS}$
		0.6674	ASt_{12}	$\omega_{fl} + 12\omega_{SRS}$
		0.6888	ASt_{11}	$\omega_{fl} + 11\omega_{SRS}$
		0.7116	ASt_{10}	$\omega_{fl} + 10\omega_{SRS}$
1.06415	$\mathbf{e}_3(\mathbf{e}_2, \mathbf{e}_2)\mathbf{e}_3$ (see Fig. 8c) [6]	0.3434	$\lambda_{S\text{-}SFM}(\lambda_{fl}, \lambda_{ASt2})$	$2\omega_{fl} + (\omega_{fl} + 2\omega_{SRS})$
		0.3490	$\lambda_{S\text{-}SFM}(\lambda_{fl}, \lambda_{ASt1})$	$2\omega_{fl} + (\omega_{fl} + \omega_{SRS})$
		0.3547	THG [7]	$3\omega_{fl}$
		0.3607	$\lambda_{S\text{-}SFM}(\lambda_{fl}, \lambda_{St1})$	$2\omega_{fl} + (\omega_{fl} - \omega_{SRS})$
		0.3668	$\lambda_{S\text{-}SFM}(\lambda_{fl}, \lambda_{St2})$	$2\omega_{fl} + (\omega_{fl} - 2\omega_{SRS})$
		0.3732	$\lambda_{S\text{-}SFM}(\lambda_{fl}, \lambda_{St3})$	$2\omega_{fl} + (\omega_{fl} - 3\omega_{SRS})$
		0.3798	$\lambda_{S\text{-}SFM}(\lambda_{fl}, \lambda_{St4})$	$2\omega_{fl} + (\omega_{fl} - 4\omega_{SRS})$
		0.3866	$\lambda_{S\text{-}SFM}(\lambda_{fl}, \lambda_{St5})$	$2\omega_{fl} + (\omega_{fl} - 5\omega_{SRS})$
		0.4102	ASt_{12}	$2\omega_{fl} + 12\omega_{SRS}$
		0.4181	ASt_{11}	$2\omega_{fl} + 11\omega_{SRS}$
		0.4264	ASt_{10}	$2\omega_{fl} + 10\omega_{SRS}$
		0.4351	ASt_9	$2\omega_{fl} + 9\omega_{SRS}$
		0.4441	ASt_8	$2\omega_{fl} + 8\omega_{SRS}$
		0.4534	ASt_7	$2\omega_{fl} + 7\omega_{SRS}$
		0.4632	ASt_6	$2\omega_{fl} + 6\omega_{SRS}$
		0.4734	ASt_5	$2\omega_{fl} + 5\omega_{SRS}$
		0.4841	ASt_4	$2\omega_{fl} + 4\omega_{SRS}$
		0.4953	ASt_3	$2\omega_{fl} + 3\omega_{SRS}$
		0.5070	ASt_2	$2\omega_{fl} + 2\omega_{SRS}$
		0.5192	ASt_1	$2\omega_{fl} + \omega_{SRS}$
		0.53207	SHG [5]	$2\omega_{fl}$
		0.5456	St_1	$2\omega_{fl} - \omega_{SRS}$
		0.5482	ASt_{19}	$\omega_{fl} + 19\omega_{SRS}$
		0.5598	St_2	$2\omega_{fl} - 2\omega_{SRS}$
		0.5625	ASt_{18}	$\omega_{fl} + 18\omega_{SRS}$
		0.5748	St_3	$2\omega_{fl} - 3\omega_{SRS}$

Table 2 (conclusion)

Pumping condition		Raman-induced nonlinear lasing		
λ_f, μm	Excitation geometry [1]	Wavelength, [2] μm	Line [3]	Nonlinear-lasing attribution [4]
		0.5777	ASt_{17}	$\omega_{fl} + 17\omega_{SRS}$
		0.5906	St_4	$2\omega_{fl} - 4\omega_{SRS}$
		0.5936	ASt_{16}	$\omega_{fl} + 16\omega_{SRS}$
		0.6073	St_5	$2\omega_{fl} - 5\omega_{SRS}$
		0.6105	ASt_{15}	$\omega_{fl} + 15\omega_{SRS}$
		0.6249	St_6	$2\omega_{fl} - 6\omega_{SRS}$
		0.6284	ASt_{14}	$\omega_{fl} + 14\omega_{SRS}$
		0.6437	St_7	$2\omega_{fl} - 7\omega_{SRS}$
		0.6473	ASt_{13}	$\omega_{fl} + 13\omega_{SRS}$
		0.6674	ASt_{12}	$\omega_{fl} + 12\omega_{SRS}$
		0.6888	ASt_{11}	$\omega_{fl} + 11\omega_{SRS}$
		0.7116	ASt_{10}	$\omega_{fl} + 10\omega_{SRS}$

[1] The notation used is analogous to that in [48].
[2] Measurement accuracy is ±0.0002 μm.
[3] St_i and ASt_i are Stokes and anti-Stokes lines; $\lambda_{S\text{-}SFM}$ corresponds to self-sum-frequency mixing, i.e., a cascaded summing parametric generation (up-conversion) process resulting from the interaction of the secondary nonlinear-laser emission (Stokes or anti-Stokes fields) and pumping radiation; for example, radiation at the wavelength $\lambda_{S\text{-}SFM}(\lambda_{fl}, \lambda_{ASt1}) = 0.3490$ μm is the result of summing interaction between two pumping photons (with the energy $2\omega_{fl} = 18794$ cm^{-1}) and a first anti-Stokes photon ($\omega_{fl} + \omega_{SRS} = 9862.5$ cm^{-1}).
[4] $\omega_{SRS} = 465.5 \pm 1$ cm^{-1} is the energy of the SRS-promoting A_1-vibration mode of the crystal.
[5] Non-phase-matchable SHG.
[6] Non-phase-matched self-frequency doubling is so strong under the experimental conditions that it gives rise to multi-wavelength cascaded SRS and RFWM around SHG. (We note that the observed lines around the SHG line may also originate from SFM of the fundamental wave and its Stokes and anti-Stokes components). For wave propagation exactly along the optic axis (the *c* axis) of the crystal, the polarization plane is rotated by optical activity (see Table 1). In our experiments, due to the use of a focused laser beam, the linear birefringence dominates the optical activity. We note that the authors of [49] did not observe the influence of optical activity in α-quartz on the SRS threshold pump intensity at temperatures below 70 K.
[7] Third harmonic generation without phase matching.

first-Stokes lasing signal for α-quartz and for a reference crystal, $PbWO_4$, with a known gain value for its $\lambda_{St1} = 1.1770$ μm wavelength [65]. We observed that the 'threshold' pump intensity for the lead tungstate reference crystal was about fifteen times less than for α-quartz. This result allows concluding that the corresponding g_{ssR}^{St1} coefficient for α-quartz is not less than 0.2 cm GW^{-1}.

5. SRS-promoting vibration mode of α-quartz

The primitive trigonal cell of α-quartz contains nine atoms with Si^{4+} ions at C_2 sites and O^{2-} ions at C_1 positions, which gives the total number $3NZ = 27$ of the vibrational degrees of freedom, which are distributed into $\Gamma_{27} = 4A_1 + 5A_2 + 9E$ irreducible representations [66]. They correspond to the two acoustic vibration branches with the $A_2 + E$ symmetry and 16 optical vibration modes with the $4A_1 + 4A_2 + 8E$ symmetry; here, the A_1 modes are Raman active, the A_2 modes are IR active, and the E vibrations are both Raman and IR active. Measured at room temperature, the energy spacing between the observed numerous Stokes and anti-Stokes lines arising from both pumping wavelengths used, λ_{fl} and λ_{f2}, as well as the energy spacing between all components of self-frequency conversion acts (doubling, tripling, cascaded generation, and

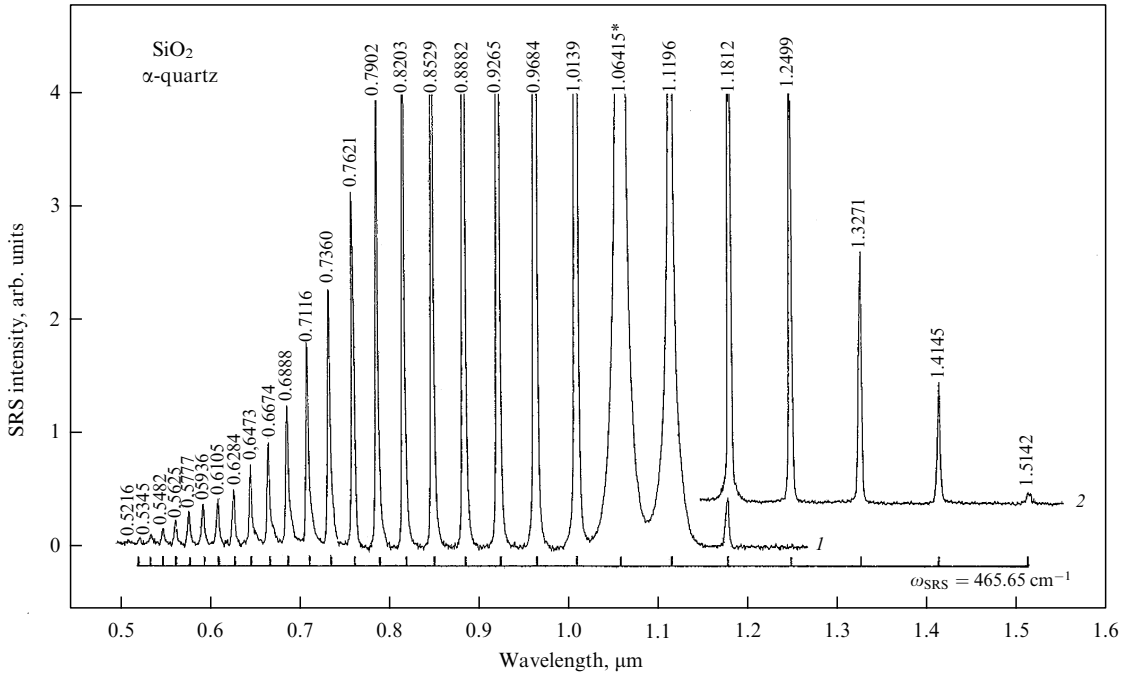

Figure 4. Room-temperature SRS and RFWM spectrum of α-quartz recorded in the excitation geometry $\mathbf{e}_1(\mathbf{e}_2, \mathbf{e}_2)\mathbf{e}_1$ under picosecond pumping at the wavelength $\lambda_{f1} = 1.06415$ μm. The wavelengths of all lines (the pump line is indicated with an asterisk) are given in μm, and their intensities are shown without correction concerning the spectral sensitivity of the analyzing CSMA system used. Detectors used: (*1*) Si-CCD and (*2*) InGaAs-CCD array sensors. The spacing of $\chi^{(3)}$-lasing components is a multiple of the SRS-promoting vibration mode ($\omega_{SRS} = 465.5$ cm^{-1}) of the crystal; it is indicated by the horizontal scale bracket.

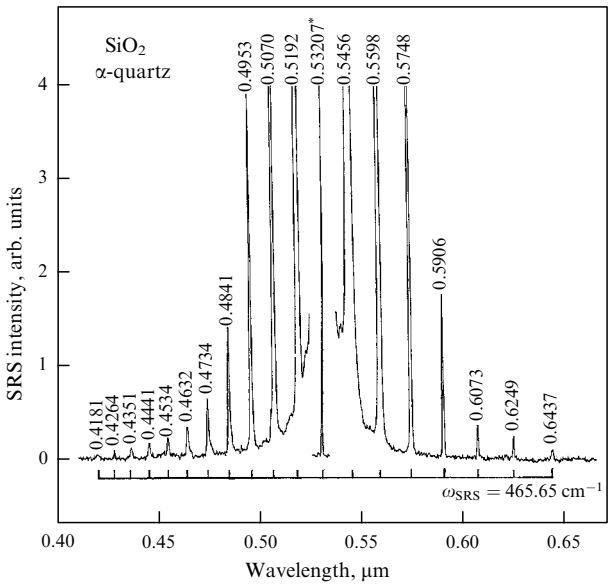

Figure 5. Room-temperature SRS and RFWM spectrum of α-quartz recorded in the excitation geometry $\mathbf{e}_1(\mathbf{e}_2, \mathbf{e}_2)\mathbf{e}_1$ under picosecond pumping at the wavelength $\lambda_{f2} = 0.53207$ μm, using an Si-CCD sensor. The notation is analogous to that in Fig. 4.

SFM with excitation at the wavelength $\lambda_{f1} = 1.06415$ μm) for single crystals of α-quartz was $\omega_{SRS} = 465.5$ cm^{-1} with high precision (see Figs 4–8). In accordance with the numerous comprehensive publications cited above (see, e.g., Refs [9, 13, 15, 45, 48]), the SRS-promoting vibration mode could be assigned to the totally symmetric internal stretching vibration A_1 mode of the silicon tetrahedra [SiO_4] of α-quartz (see Fig. 9).

6. Conclusion

Basic research on SRS over the last decade shows that Raman-induced cascaded frequency conversion phenomena in crystalline materials offer very promising possibilities that allow substantially enriching the arsenal of efficient light sources for modern laser physics and nonlinear optics. The results of numerous experiments that have been carried out in this attractive field of investigations (see, e.g., [46, 56, 62, 63, 67, 68]) show that for each new SRS-active crystal (both centrosymmetric and noncentrosymmetric), new properties of the observed nonlinear-laser processes occur, which may open the way to novel optical technologies. In particular, the observed ultra-broadband Stokes and anti-Stokes optical comb lasing is of special interest for achieving different femtosecond waveforms and nonsinusoidal light. We expect that α-quartz, with the discovered lasing combs of more than two-octave bandwidth and its well-known unique physical, optical, and nonlinear-laser properties, will be among the crystals of choice for such tempting applications.

An important point to note is that all the new manifestations of nonlinear laser processes in α-quartz that we have discovered are based on the Raman scattering in this crystal, discovered by Landsberg and Mandelshtam 80 years ago [7]. Commemorating this scientific benchmark, we have decided to dedicate this paper to the anniversary of that great discovery. We join the majority of scientists in expressing our regret that Landsberg and Mandelshtam were not awarded a Nobel prize for their truly remarkable discovery [69, 70]. The published archives of the Nobel Committee reveal that that was a mistake [71, 72]. After the lapse of 80 years, the true magnitude of this discovery is more evident than ever.

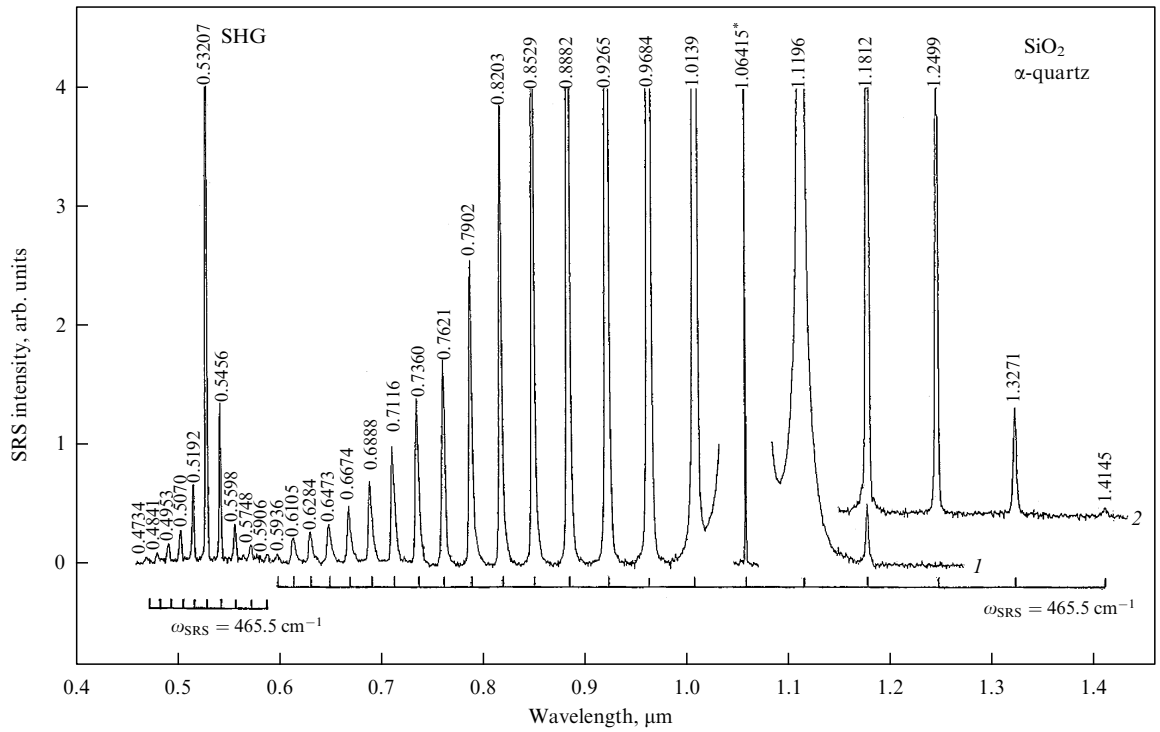

Figure 6. The room-temperature SRS and RFWM spectrum of α-quartz recorded in the excitation geometry $\mathbf{e}_2(\mathbf{e}_1, \mathbf{e}_1)\mathbf{e}_2$ under picosecond pumping at the wavelength $\lambda_{f1} = 1.06415$ μm using an Si-CCD (*1*) and an InGaAs-CCD (*2*) sensor (see Table 2).The spacing of $\chi^{(3)}$- and cascaded self-frequency doubling $\chi^{(3)} \leftrightarrow \chi^{(2)}$-lasing components is a multiple of the SRS-promoting vibration mode ($\omega_{SRS} = 465.5$ cm^{-1}) of the crystal; it is indicated by the horizontal scale brackets. The notation is analogous to that in Fig. 4.

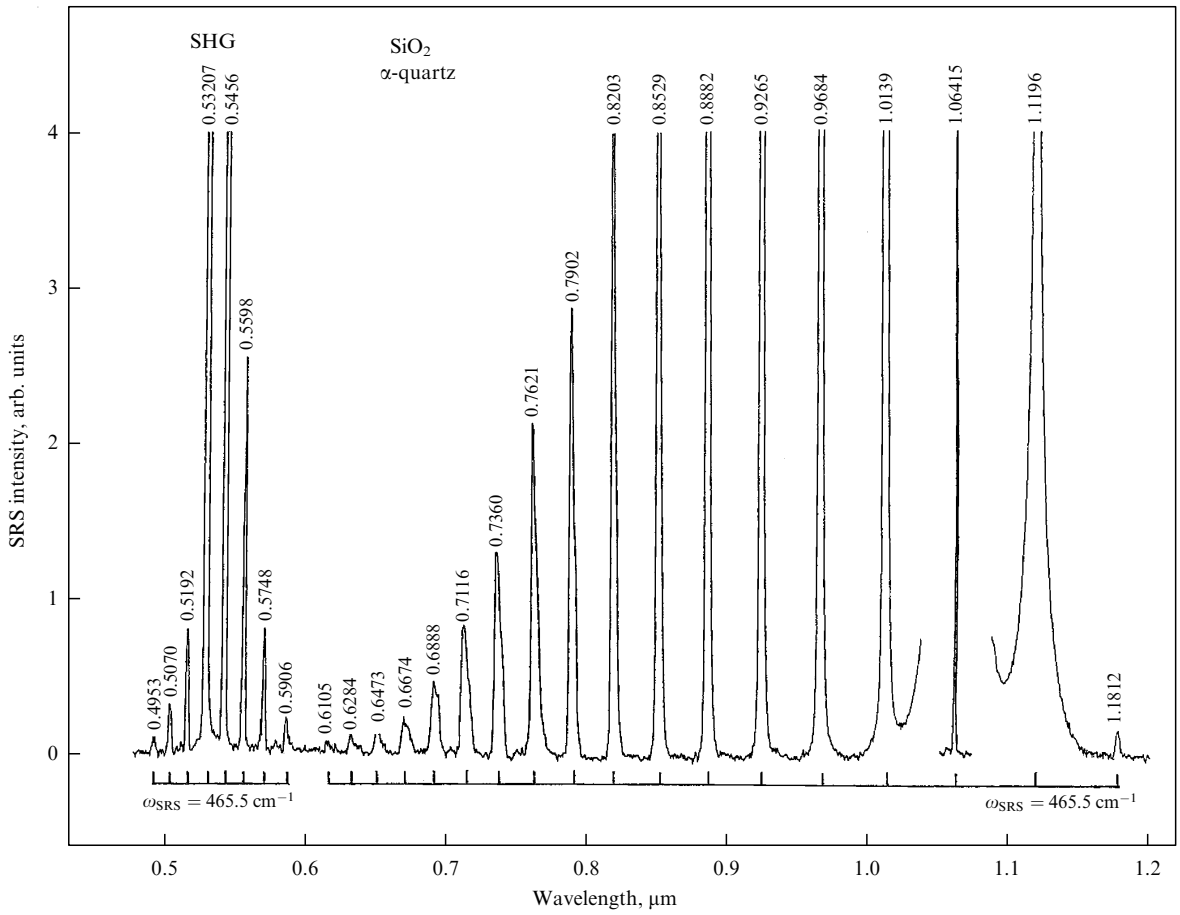

Figure 7. The room-temperature SRS and RFWM spectrum of α-quartz recorded in the excitation geometry $\mathbf{e}_3(\mathbf{e}_2, \mathbf{e}_2)\mathbf{e}_3$ under picosecond pumping at the wavelength $\lambda_{f2} = 0.53207$ μm using an Si-CCD sensor (see Table 2). The notation is analogous to that in Figs 4 and 5.

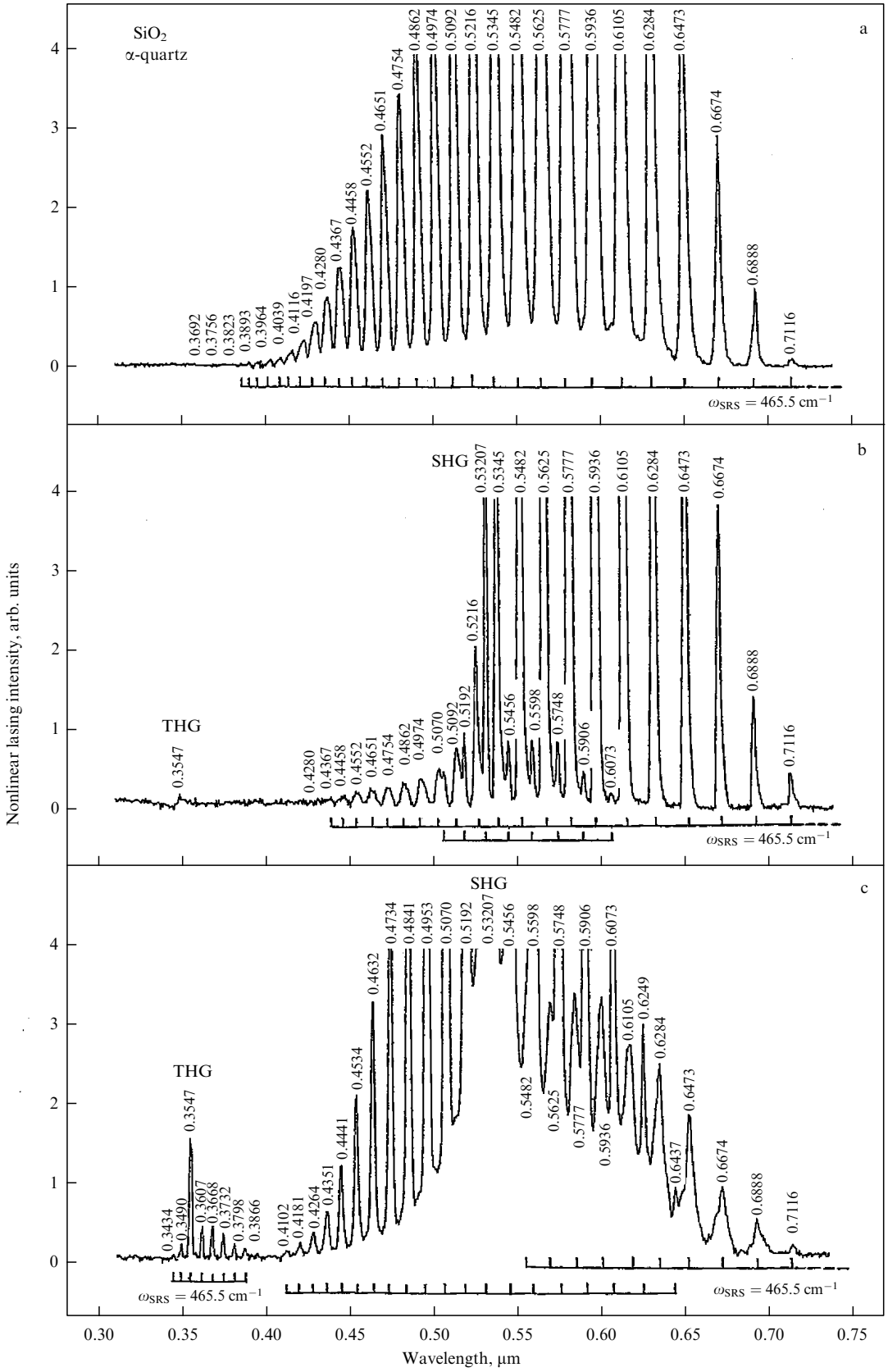

Figure 8. Room-temperature SRS and RFWM spectra of α-quartz recorded under picosecond pumping at the wavelength $\lambda_{fl} = 1.06415$ μm using an Si-CCD sensor (see text and Table 2) in the excitation geometries $\mathbf{e}_1(\mathbf{e}_2, \mathbf{e}_2)\mathbf{e}_1$ (a), $\mathbf{e}_2(\mathbf{e}_1, \mathbf{e}_1)\mathbf{e}_2$ (b), and $\mathbf{e}_3(\mathbf{e}_2, \mathbf{e}_2)\mathbf{e}_3$ (c). All these spectra were obtained under special experimental conditions. The spacing of SRS cascaded self-frequency doubling and tripling components is a multiple of the $\chi^{(3)}$-active vibration mode ($\omega_{SRS} = 465.5$ cm^{-1}) of the crystal. The notation is analogous to that in Figs 4 and 5.

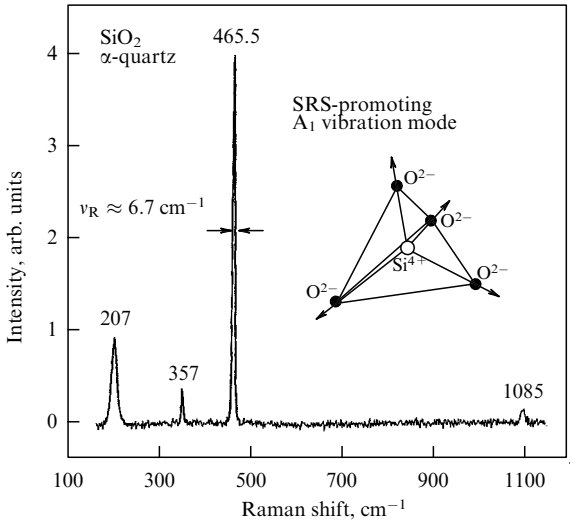

Figure 9. Section of a room-temperature spontaneous Raman scattering spectrum (A_1-modes) of α-quartz (see, e.g., Refs [45, 48]). The frequencies of Raman-shifted lines are given in cm^{-1}. The inset shows the totally symmetric internal stretching vibration A_1-mode of the silicon tetrahedra [SiO_4] of α-quartz.

Acknowledgments

The research was supported in part by the Russian Foundation for Basic Research and the Femtosecond Physics and New Optical Materials Program of the Presidium of the Russian Academy of Sciences, as well as by the University of Cologne and by the Technical University of Berlin. A.A.K. is grateful to the Alexander von Humboldt Foundation for the Festkörperphysik Research Prize, which allowed him to carry out SRS experiments at the Institute of Optics and Atomic Physics of the Technical University of Berlin. He is also thankful to I L Fabelinskii for the numerous conversations on the history of the discovery and pioneering works in Russia on light scattering in α-quartz by Landsberg and Mandelshtam. The authors note that progress in the present work was made possible by cooperation within the Joint Open Laboratory for Laser Crystals and Precise Laser Systems. The authors also thank C Scharfenorth for spectroscopic experimental help and M Mühlberg for large pieces of a synthetic crystal of α-quartz.

References

1. Arago F *Mém. Classe Sci. Math. Phys. Inst.* (1) 115 (1811)
2. Fresnel A *Ann. Chim. Phys.* **28** 147 (1825)
3. Brewster D *Philos. Trans. R. Soc. London* **105** 60 (1815)
4. Brewster D *Trans. R. Soc. Edinb.* **8** 281, 369 (1818)
5. Röntgen W C *Wied. Ann.* **18** 213 (1883); Kundt A *Wied. Ann.* **18** 228 (1883); Röntgen W C *Wied. Ann.* **18** 534 (1883); **19** 319 (1883)
6. Pockels F *Abhandl. Ges. Wiss. Göttingen Math. Phys. Kl.* **39** 1 (1894)
7. Landsberg G, Mandelstam L *Naturwissenschaften* **16** 557 (1928); *Z. Phys.* **50** 769 (1928)
8. Raman C V *Ind. J. Phys.* **2** 387 (1928); Raman C V, Krishnan K S *Ind. J. Phys.* **2** 399 (1928); Krishnan K S *Nature* **122** 477 (1928)
9. Rao I R *Ind. J. Phys.* **3** 123 (1928); Landsberg G, Leontovich M *Z. Phys.* **53** 439 (1929); Landsberg G, Wulfsohn K *Z. Phys.* **58** 95 (1929); Krishnan K S *Ind. J. Phys.* **4** 131 (1929); Gross E, Romanova M *Z. Phys.* **55** 744 (1929); Kujumzelis Th G *Z. Phys.* **100** 221 (1936); Saksena B D *Proc. Ind. Acad. Sci. A* **16** 270 (1942); Krishnan R S *Nature* **155** 452 (1945); Krishnamurti D *Proc. Ind. Acad. Sci. A* **47** 276 (1958)
10. Franken P A et al. *Phys. Rev. Lett.* **7** 118 (1961)
11. Charra F, Gurzadyan G G, in *High Frequency Properties of Dielectric Crystals*: *Nonlinear Dielectric Susceptibilities* (Landolt-Börnstein, New Series, Group III, Vol. 30b, Ed. D F Nelson) (Berlin: Springer, 2000) p. 44
12. Roberts D A *IEEE J. Quantum Electron.* **28** 2057 (1992)
13. Tannenwald P E, Thaxter J B *Science* **154** 1319 (1966); Tannenwald P, Weinberg D L *IEEE J. Quantum Electron.* **3** 334 (1967)
14. Chiao R Y, Townes C H, Stoicheff B P *Phys. Rev. Lett.* **12** 592 (1964); Krivokhizha S V et al. *Pis'ma Zh. Eksp. Teor. Fiz.* **3** 378 (1966) [*JETP Lett.* **3** 245 (1966)]
15. Shapiro S M, Axe J D *Phys. Rev. B* **6** 2420 (1972); Striefler M E, Barsch G R *Phys. Rev. B* **12** 4553 (1975); Grimsditch M H et al. *Phys. Rev. B* **15** 5869 (1977); Gale G M, Laubereau A *Opt. Commun.* **44** 273 (1983)
16. Biraud-Laval S, Chartier G *Phys. Lett. A* **30** 177 (1969); Biraud-Laval S et al. *Phys. Rev. B* **13** 1797 (1976)
17. Wilke K-Th, Bohm J *Kristallzüchtung* (Berlin: VEB Deutscher Verlag der Wissenschaften, 1988) p. 1046 ff. and references therein
18. Schafhäutl K E *Bull. Königl. Akad. Wiss.* (20) 501 (1845); *Gelehrte Anzeigen Bayer. Akad. Wiss.* (72) (10. April 1845)
19. Bragg W H, Gibbs R E *Proc. R. Soc. London A* **109** 405 (1925)
20. de Vries A *Nature* **181** 1193 (1958)
21. Donnay J D H, Le Page Y *Acta Cryst. A* **34** 584 (1978)
22. *IEEE Standard on Piezoelectricity, an American National Standard,* Std 176-1987 (New York: IEEE Standards Board, American National Standards Institute, 1988)
23. Kern A, Eysel W *Z. Kristallogr.* **198** 177 (1992)
24. Batuecas T *Nature* **159** 705 (1947)
25. Chase M W (Jr.) (Ed.) *NIST-JANAF Thermochemical Tables* 4th ed. (Gaithersburg: National Institute of Standard and Technology, 1998)
26. Mackenzie J D *J. Am. Ceram. Soc.* **43** 615 (1960)
27. Haussühl S *Kristallphysik* (Weinheim: Physik-Verlag, Verlag Chemie, 1983)
28. Dmitriev V G, Gurzadyan G G, Nikogosyan D N *Handbook of Nonlinear Optical Crystals* 2nd ed. (Berlin: Springer, 1997)
29. Tan G L et al. *Phys. Rev. B* **72** 205117 (2005)
30. Draggoo V et al. *IEEE J. Quantum Electron.* **8** 54 (1972)
31. Frondel C *The System of Mineralogy* Vol. III *Silica Minerals* (New York: Wiley, 1962) p. 129
32. Kizel' V A, Burkov V I *Girotropiya Kristallov* (Gyrotropy of Crystals) (Moscow: Nauka, 1980)
33. Adair R, Chase L L, Payne S A *Phys. Rev. B* **39** 3337 (1989)
34. Crane G R, Bergman J G *J. Chem. Phys.* **64** 27 (1976)
35. Bohatý L *Z. Kristallogr.* **161** 299 (1982)
36. Narasimhamurty T S *J. Opt. Soc. Am.* **59** 682 (1969)
37. Fontanella J, Andeen C, Schuele D *J. Appl. Phys.* **45** 2852 (1974)
38. Barron T H K et al. *J. Phys. C*: *Solid State Phys.* **15** 4311 (1982)
39. Spitzer F "Die Bestimmung der piezoelektrischen Moduln einiger isomorpher Kristalle", Dissertation (Göttingen: Univ. Göttingen, 1938)
40. Bhalla A S, Cook W R, Liu S T, in *Low Frequency Properties of Dielectric Crystals. Piezoelectric, Pyroelectric, and Related Constants* (Landolt-Börnstein, New Series, Group III, Vol. 29b, Ed. D F Nelson) (Berlin: Springer, 1993) p. 141
41. James B J, in *Proc. of the 42nd Annual Symp. on Frequency Control* (New York: IEEE, 1988) p. 146
42. Okhotin A S et al. *Teploprovodnost' Tverdykh Tel* (Heat Conductivity of Solids) (Ed. A S Okhotin) (Moscow: Energoatomizdat, 1984); Beasley J D *Appl. Opt.* **33** 1000 (1994)
43. Every A G, McCurdy A K, in *Low Frequency Properties of Dielectric Crystals. Second and Higher Order Elastic Constants* (Landolt-Börnstein, New Series, Group III, Vol. 29a, Ed. D F Nelson) (Berlin: Springer, 1992) p. 148
44. Zubov V G, Osipova L P *Kristallogr.* **6** 418 (1961) [*Sov. Phys. Crystallogr.* **6** 330 (1961)]; Tannenwald P E *J. Appl. Phys.* **38** 4788 (1967); Pine A S, Tannenwald P E *Phys. Rev.* **178** 1424 (1969); Harker Y D, She C Y, Edwards D F *Appl. Phys. Lett.* **15** 272 (1969); Ichikawa S et al. *J. Raman Spectrosc.* **34** 135 (2003)
45. Scott J F *IEEE J. Quantum Electron.* **3** 693 (1967); Fabelinskii I L, Starunov V S *Appl. Opt.* **6** 1793 (1967) and references therein; Aref'ev I M et al. *Pis'ma Zh. Eksp. Teor. Fiz.* **8** 142 (1968) [*JETP*

Lett. **8** 84 (1968)]; Pine A S, Dresselhaus G *Phys. Rev*. **188** 1489 (1969); Klein M, Maier M *Opt. Commun*. **44** 411 (1983)
46. Kaminskii A A et al. *Laser Phys. Lett*. **5** 532 (2008)
47. Kaminskii A A *Zh. Eksp. Teor. Fiz*. **51** 49 (1966) [*Sov. Phys. JETP* **24** 33 (1967)]; *Laser Crystals*: *Their Physics and Properties* (Berlin: Springer-Verlag, 1981, 2nd ed. — 1990)
48. Damen T C, Porto S P S, Tell B *Phys. Rev*. **142** 570 (1966); Scott J F, Porto S P S *Phys. Rev*. **161** 903 (1967)
49. Klein M, Maier M, Prettl W *Phys. Rev. B* **28** 6008 (1983)
50. Kaminskii A A, Bohatý L, Becker P *Ferroelectrics* **352** 42 (2007)
51. Kaminskii A A et al. *J. Raman Spectrosc*. **29** 645 (1998)
52. Kaminskii A A et al. *Dokl. Ross. Akad. Nauk* **367** 464 (1999) [*Dokl. Phys*. **44** 495 (1999)]
53. Kaminskii A A, Hulliger J, Eichler H J *Phys. Status Solidi A* **186** R19 (2001)
54. Kaminskii A A et al. *Opt. Commun*. **206** 179 (2002)
55. Kaminskii A A et al. *Jpn. J. Appl. Phys*. **41** L603 (2002)
56. Kaminskii A A et al. *Laser. Phys*. **13** 1385 (2003)
57. Kaminskii A A et al. *Phys. Status Solidi A* **201** 3200 (2004)
58. Becker P et al. *Phys. Status Solidi A* **202** 2543 (2005)
59. Bohatý L et al. *Laser Phys*. **15** 1509 (2005)
60. Kaminskii A A et al. *Laser Phys. Lett*. **3** 519 (2006)
61. Kaminskii A A et al. *Laser Phys. Lett*. **4** 660 (2007)
62. Becker P et al. *Laser Phys. Lett*. **5** 114 (2008)
63. Hakuta K et al. *Phys. Rev. Lett*. **79** 209 (1997); Zhi M, Sokolov A V *Opt. Lett*. **32** 2251 (2007)
64. Shen Y R *The Principles of Nonlinear Optics* (New York: J. Wiley, 1984) [Translated into Russian (Moscow: Nauka, 1989)]
65. Kaminskii A A et al. *Opt. Commun*. **183** 277 (2000)
66. Saksena B D *Proc. Ind. Acad. Sci. A* **12** 93 (1940); Rousseau D L, Bauman R P, Porto S P S *J. Raman Spectrosc*. **10** 253 (1981)
67. Kaminskii A A et al. *Laser Phys. Lett*. **4** 668 (2007)
68. Kaminskii A A et al. *Laser Phys. Lett*. **5** 304 (2008)
69. Fabelinskii I L *Usp. Fiz. Nauk* **168** 1341 (1998) [*Phys. Usp*. **41** 1229 (1998)]
70. Fabelinskii I L *Usp. Fiz. Nauk* **173** 1137 (2003) [*Phys. Usp*. **46** 1105 (2003)]
71. Ginzburg V L *Vestn. Ross. Akad. Nauk* **68** 51 (1998) [*Herald Russ. Acad. Sci*. **68** 56 (1998)]
72. Ginzburg V L, Fabelinskii I L *Vestn. Ross. Akad. Nauk* **73** 215 (2003) [*Herald Russ. Acad. Sci*. **73** 152 (2003)]